Characteristics of plasma scalds in multilayer dielectric films

Xiaofeng Liu,[1] Yuan'an Zhao,[1,*] Dawei Li,[1] Guohang Hu,[1] Yanqi Gao,[2] Zhengxiu Fan,[1] and Jianda Shao[1]

[1]Key Laboratory of High Power Laser Materials, Shanghai Institute of Optics and Fine Mechanics, Shanghai 201800, China

[2]Shanghai Institute of Laser Plasma, Shanghai 201800, China

*Corresponding author: yazhao@siom.ac.cn

Received 22 February 2011; accepted 20 May 2011;
posted 22 June 2011 (Doc. ID 143050); published 19 July 2011

Plasma scalding is one of the most typical laser damage morphologies induced by a nanosecond laser with a wavelength of 1053 nm in HfO_2/SiO_2 multilayer films. In this paper, the characteristics of plasma scalds are systematically investigated with multiple methods. The scalding behaves as surface discoloration under a microscope. The shape is nearly circular when the laser incidence angle is close to normal incidence and is elliptical at oblique incidence. The nodular-ejection pit is in the center of the scalding region when the laser irradiates at the incidence angle close to normal incidence and in the right of the scalding region when the laser irradiates from left to right at oblique incidence. The maximum damage size of the scalding increases with laser energy. The edge of the scalding is high compared with the unirradiated film surface, and the region tending to the center is concave. Plasma scald is proved to be surface damage. The maximum depth of a scald increases with its size. Tiny pits of nanometer scale can be seen in the scalding film under a scanning electronic microscope at a higher magnification. The absorptions of the surface plasma scalds tend to be approximately the same as the lower absorptions of test sites without laser irradiation. Scalds do not grow during further illumination pulses until 65 J/cm^2. The formation of surface plasma scalding may be related to the occurrence of the laser-supported detonation wave.

OCIS codes: 140.3330, 240.0310, 310.1620.

1. Introduction

1053 nm highly reflective coatings with high laser-induced damage thresholds (LIDTs) are required for high power lasers. It is well established that the material combination that consistently exhibits a high damage thresholds is HfO_2/SiO_2 [1,2]. However, exposed to laser fluence as high as 30 J/cm^2 (in 3 ns pulses) [3], the mirrors do not avoid being damaged due to the presence of defects. Plasma scalding, associated with the observation by eye of plasma luminescence, is one of the most typical damage morphologies in laser damage and laser conditioning [4–7]. A damage diagnostic system for collecting plasma flashes was developed to detect such damage in LIDT tests [8]. Previous studies showed that it behaved as surface discoloration under a microscope and exhibited a different contrast compared with the undamaged surface under scanning electronic microscope (SEM) [4,5]. Pairs of dependent or independent scalds were induced by one shot after 1-on-1 testing in a previous study [5]. A pit that proved to be a nodular-ejection or flat bottom pit was always seen in a scald [5,9]. The diameter of the scald was found to increase almost linearly with the fluence [4]. Some experiments have also shown that the size increases with longer pulse duration [10].

For the purpose of increasing the understanding of plasma scalding damage and providing exact

0003-6935/11/214226-06$15.00/0

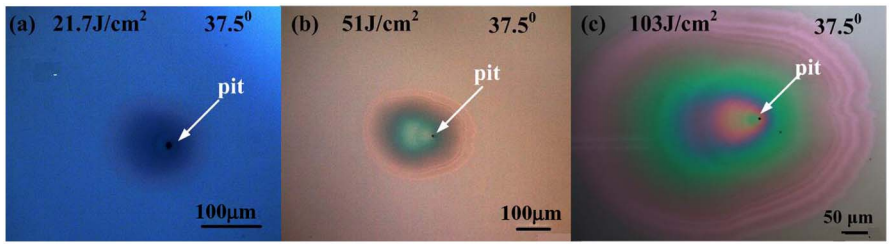

Fig. 1. (Color online) Microscope micrograms of plasma scalds after one shot.

evidence for theoretical studies, this article will focus on characterizing the plasma scalding damage induced by nanosecond laser pulses found in HfO_2/SiO_2 multilayer mirrors. Microscope, SEM, step profiler, atomic force microscope (AFM), and surface thermal lensing (STL) measurement are used to analyze plasma scalds. The mechanisms of the scald morphology formation are discussed based on the experimental results.

2. Experiments

A. Sample Preparations

The mirrors were prepared by electron-beam deposition from hafnia and silica starting materials onto BK7 substrates. All coating runs used the same deposition technology and were in the same coating chamber. They all had silica overcoats and reflected highly at a wavelength of 1064 nm and an incidence angle of 37.5°. The thickness of the silica outer layer was about 988 nm.

B. Experimental Details

1. *Damage Experiments*

The laser damage system used was introduced in Ref. [11]. Laser damage experiments were carried out using a 9 ns pulse from a 1064 nm Nd: YAG laser at a 37.5° incidence angle with "S" polarization. The effective area of the spot was 0.42 mm^2 at normal incidence. The distance between two neighboring test sites was 90% of the beam's effective diameter. The lasma luminescence detection system introduced in Ref. [8] was used to determine the plasma scalding damage.

2. *Analysis Methods*

A Leica microscope was used to observe the surface morphology of the plasma scalding. An Alpha-Step 500 surface profiler, with a resolution of step heights down to 50 Å through a scanning length of 10 mm maximum, was used to detect the depth information of the whole plasma scalding region. A Zeiss SEM with nanometer horizontal resolution was used to observe the surface morphology of microareas. A VEECO Dimension 3100 AFM with nanometer horizontal and vertical resolution was used to obtain the microarea surface roughness profile information. The weak absorption detection setup based on the STL technique in Ref. [12] was used to evaluate the absorptions of scalds and unirradiated films.

3. Results

A. The Morphology Characteristics of Plasma Scalds

1. *Macrocharacteristics of Plasma Scalds*

Scalding behaves as surface discoloration under a microscope as shown in Fig. 1, and several obvious ripples appear in the periphery of the severe scald [see Fig. 1(c)]. Plasma luminescence corresponds to scalding with an elliptical shape in our experiments. In our previous experiments, the shape of the scalding was nearly circular with laser irradiation at a near-normal incidence angle [5] and was elliptical when the incidence angle of the laser was 45° [9].

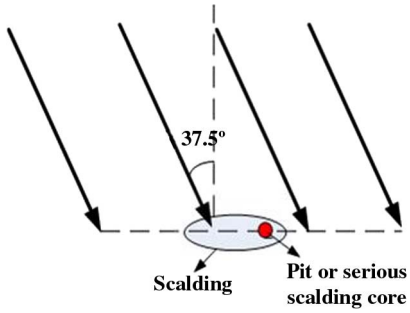

Fig. 2. (Color online) Incident direction of the laser and the location of the pit in our experiments.

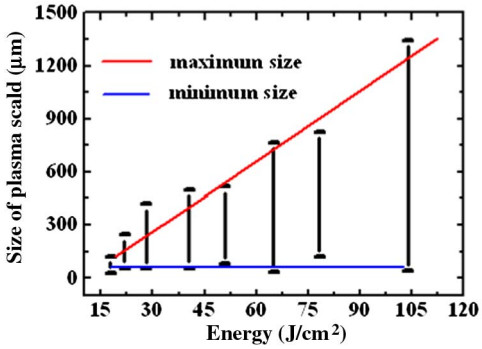

Fig. 3. (Color online) Size distribution of scalds versus energy of the irradiation laser.

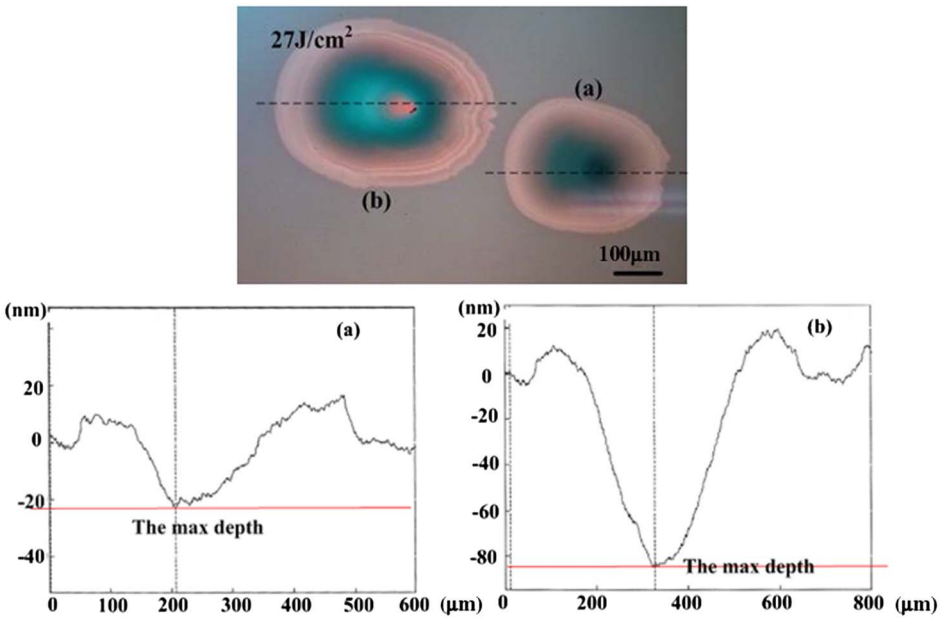

Fig. 4. (Color online) Surface profiler results of plasma scalds. (a), (b) The surface profiler results of the plasma scalds marked by (a) and (b) in the top figure. The probe of the surface profiler moves along the dotted line shown in the top figure.

These phenomena indicate that the shape of the scalding shows a relationship with the laser incidence angle. It tends to be circular when the laser irradiates at a near-normal incidence angle and to be elliptical for oblique incidence. The shape of the scalding is similar to the shape of the laser spot. However, it is not definite that all of these scalds are located at the peak region of the Gaussian intensity profile of the laser beam, and one cannot draw the conclusion that the shape of the scalding has something to do with the spot shape. The pit is not located at the center of the scald for oblique incidence as it is for near-normal incidence in Ref. [5]. It is in the right part of a scald as observed from the front surface when the laser irradiates at an oblique incidence as shown in Fig. 2.

Figure 3 is the size distribution of scalds versus energy of the irradiation laser. The size of the elliptical scald is defined as its major axis. Twenty random scalds are observed at one energy step. The sizes of the scalds range from tens of micrometers to hundreds of micrometers below $80\,\mathrm{J/cm^2}$ to more than 1 mm at $103\,\mathrm{J/cm^2}$. Figure 3 illustrates that the minimum scalding size is around $50\,\mu\mathrm{m}$, and the maximum scalding size increases with the energy.

The step profiler micrograms of plasma scalds and the definition of their maximum depths are shown in Fig. 4. It is found that the edge of the scalding is high compared with the undamaged film surface, and the region tending to the center is concave. The maximum depths of scalds range from 6 nm to more than 100 nm in our samples (Fig. 5). The maximum depth of a severe scald is nearly 180 nm in our measurements, and it is much less than the thickness of the SiO_2 outer layer. The maximum depths of the scalds exhibit an obvious relation with the scalding size. The statistical data reveals that the maximum depth increases with the size of the scald (Fig. 5).

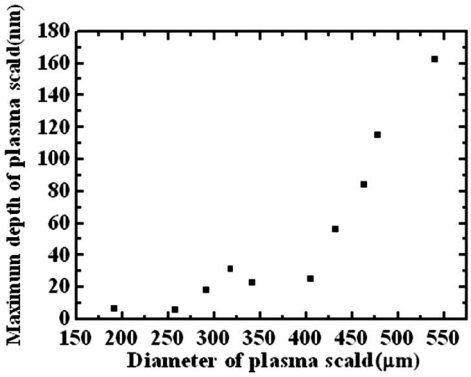

Fig. 5. Maximum depth of a plasma scald versus its maximum size.

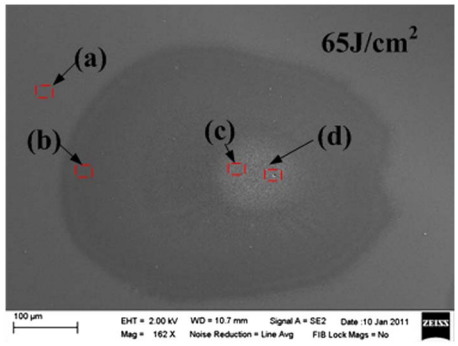

Fig. 6. (Color online) SEM microgram of the plasma scald; microareas (a), (b), (c), and (d) are observed at a higher magnification in Fig. 7.

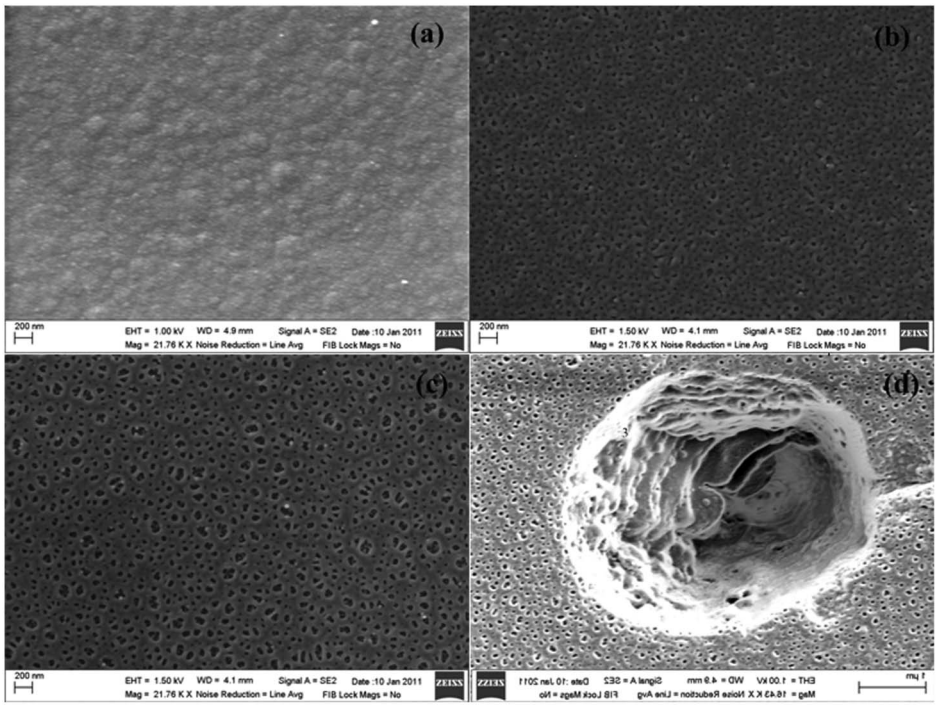

Fig. 7. (a)(d) Local views of (a), (b), (c), and (d), marked by rectangles, in Fig. 6.

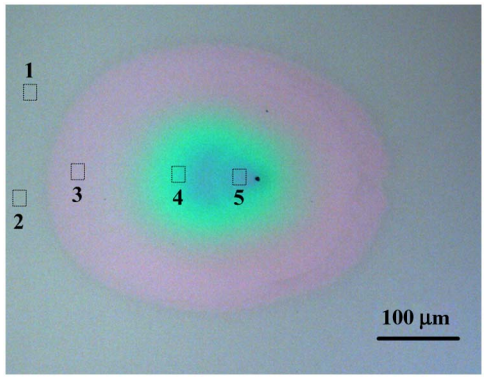

Fig. 8. (Color online) Microareas chosen for RMS roughness test. Regions 1 and 2 are undamaged regions; regions 3, 4, and 5 are microareas in the scalding region.

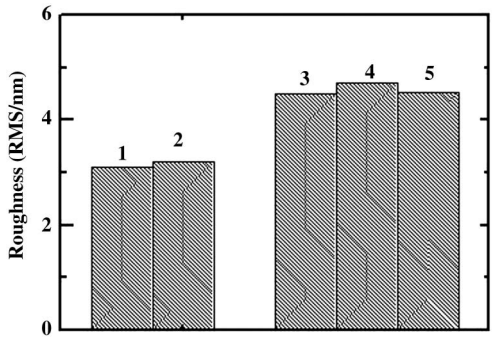

Fig. 9. RMS roughness results of the microareas marked by rectangles 1, 2, 3, 4, and 5 in Fig. 8.

2. *Microcharacteristics of Plasma Scalds*

The picture in Fig. 6 is the SEM micrograph of a scald. The local magnified views of areas (a)–(d) of Fig. 6, marked by rectangles, are shown in Figs. 7(a)–7(d). Figure 7(a) is the SEM micrograph of undamaged film, and Fig. 7(d) is the SEM micrograph of the pit in the scalding region.

The scalding region shows a different contrast compared with the film surface under SEM as observed in previous studies [5,9]. Compared with undamaged film [see Fig. 7(a)], many tiny pits of nanometer scale can be seen at a higher magnification [see Figs. 7(b)–7(d)]. The sizes of these tiny pits in Fig. 7(c) are larger than in Fig. 7(b). The pit in the scald is a nodular-ejection pit of micrometer size [see Fig. 7(d)].

Microareas shown in Fig. 8 are chosen for RMS roughness study. Regions 1 and 2 are undamaged regions; regions 3, 4, and 5 are microareas in the scalding region. AFM results in Fig. 9 show that the RMS roughness of the scalding region increases compared with the film surface without laser irradiation. The RMS roughness of the film surface is about 3.1 nm, and the RMS roughness of the scalding regions is approximately 4.5 nm.

B. The Absorption Characteristics of Plasma Scalds

Absorptions of 20 plasma scalding areas and unirradiated areas are measured, respectively. Absorption in each area is measured ten times, and the average absorption value of each area is obtained. The average absorption result given in Fig. 10 indicates that several strong absorption sites appear in the coating

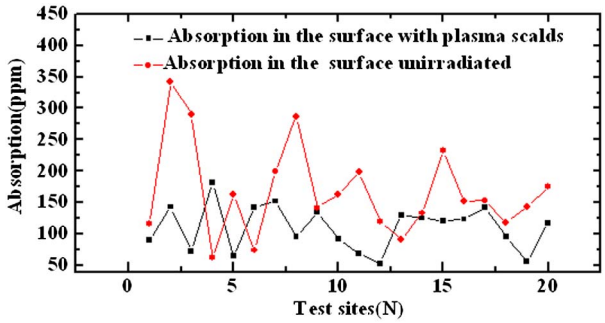

Fig. 10. (Color online) Absorptions of scalds and unirridiated film.

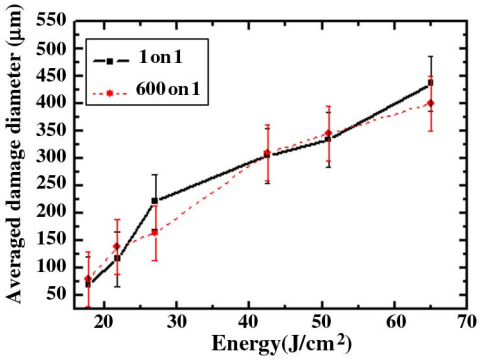

Fig. 11. (Color online) Average diameters of scalds as a function of irradiated energy after 1 shot and 600 shots.

without laser irradiation. It is also found that the absorptions of the surface plasma scalds tend to be approximately the same as the lower absorptions of test sites without laser irradiation.

C. The Damage Characteristics of Scalds after Multiple Shots

The statistical average damage size of the scalds is shown in Fig. 11. It illustrates that the scald is not aggravated after 600 shots and up to 65 J/cm^2 in fluence, which is the maximum energy step used in our experiments. The damage morphologies of scalds after one shot and multiple shots are shown in Fig. 12, and no obvious and essential change is found.

4. Discussion

Laser and material interaction is a complex process. No further explanations for plasma scalds are reported, except that they are initiated at defects, contaminations, or air breakdown during a laser shot and are caused by an increase of temperature on the surface during plasma formation [13]. The nodular-ejection pit shown in Fig. 7(d) proves that nodular defects play an important role in the initiation of scalding. A nodular defect tends to focus light [14] within the defect, and the average temperature of a nodular defect easily rises to several thousand degrees [15]. Therefore, a nodular defect behaves as an ejection source during laser irradiation.

Scalds exhibit an obvious relationship with laser incidence direction in our experiments, which

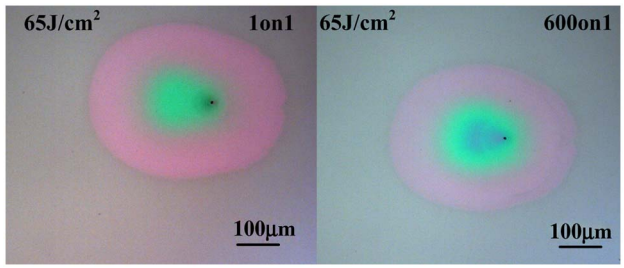

Fig. 12. (Color online) Typical damage morphologies of the plasma scald in the film surface after 1 shot and 600 shots.

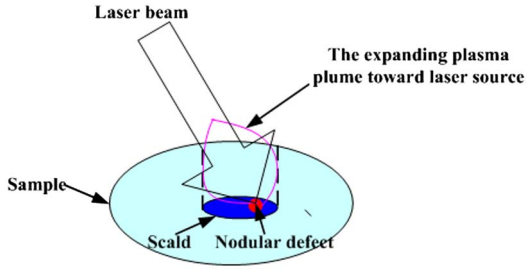

Fig. 13. (Color online) Shape of the region contaminated by the ejections.

implies that this phenomenon may be correlated to laser-supported detonation waves (LSDWs). It is believed that plasmas can absorb incoming laser energy and generate a self-sustained LSDW. LSDWs typically occur at a laser intensity that is higher than 100 GW/m^2 and usually move toward the radiation source [16,17]. For a Gaussian laser with a pulse duration of 9 ns and an effective area of 0.42 mm^2, when energy reaches 0.1 J/cm^2, the peak intensity of the laser approximates 100 GW/m^2. It is easy to reach the ignition threshold of LSDW as long as a certain density of plasma is formed in advance. A possible explanation for plasma scald originating from a nodular defect is put forward on this basis.

During a laser shot, nodular ejection usually happens in the first few nanoseconds. Generally, theses superheated ejections are partially ionized. They will be heated to ionize further and generate plasmas in the subsequent several nanoseconds. The expanding plasma plume, with neutral atoms, molecules, ions, electrons, and so on, propagates along the direction of the laser incidence and forms LSDWs [18]. Part of the ejections inevitably redeposit on the film surface. Because the moving direction of ejections is along the direction of the laser incidence, the region where ejections redeposit is elliptical, with the pit in its right part, for oblique incidence based on the projection theorem (see Fig. 13). For near-normal incidence, the ejections redeposit around the pit. The whole contaminated region, acting as a large absorbing region, will be heated to a high temperature because of contact with the high temperature plasma plume or being irradiated by the end of the pulse. The materials will be evaporated, resulting in surface damage. These scattered ejections behave as tiny absorbing points. The points, where scattered

ejections exist, will be melted and heated to a higher temperature. More materials are evaporated and form tiny pits, as shown in the locations in Figs. 7(b) and 7(c).

5. Conclusion

1. The scalding behaves as surface discoloration under a microscope. The shape is nearly circular when the incidence angle is close to normal incidence, and it is elliptical at oblique incidence. The nodular-ejection pit is in the center of scalding region when the laser irradiates at the incidence angle close to normal incidence, and it is in the right of the scalding region when the laser irradiates from left to right at oblique incidence. The maximum damage diameter of scalding increases with the incident laser energy. The edge of the scalding is high compared with the undamaged film surface, and the region tending to the center is concave. The maximum depth of a scald increases with its size.

2. Scalding exhibits a different contrast compared with the unirradiated surface. Many tiny pits of nanometer scale can be seen at a higher magnification. The RMS roughness of the film surface is about 3.1 nm and the RMS roughness of the scalding region is approximately to 4.5 nm.

3. The absorptions of the surface plasma scalds tend to be approximately the same as the lower absorptions of test sites without laser irradiation, and no high absorption, as occurs in the unirriadiated film, is observed.

4. Scalds do not grow by pulses up to a fluence of $65\,J/cm^2$.

5. The formation of the scalding morphology may be related to LSDWs, which is inferred from our experimental results.

This work is supported by the National Natural Science Foundation of China (NSFC) (60878045).

References

1. C. Fournet, B. Pinot, B. Geenen, F. Ollivier, W. Alexandre, H. G. Floch, A. Roussel, C. Cordillot, and D. Billon, "High damage threshold mirrors and polarizers in the ZrO_2/SiO_2 and HfO_2/SiO_2 dielectric system," Proc. SPIE **1624**, 282–293 (1992).
2. C. J. Stolz, M. D. Thomas, and A. J. Griffin, "BDS thin film damage competition," Proc. SPIE **7132**, 71320C (2008).
3. R. Chow, M. Runkel, and J. R. Taylor, "Laser damage testing of small optics for the National Ignition Facility," Appl. Opt. **44**, 3527–3531 (2005).
4. F. Y. Génin, and C. J. Stolz, "Morphologies of laser-induced damage in hafnia-silica multilayer mirror and polarizer coatings," Proc. SPIE **2870**, 439–448 (1996).
5. X. F. Liu, X. Li, D. W. Li, Y. A. Zhao, and J. D. Shao, "1064 nm laser conditioning effect of HfO_2/SiO_2 high reflectors deposited by e-beam," Chin. J. Laser. **36**, 1545–1549 (2009) (in Chinese).
6. L. Sheehan, M. Kozlowski, and B. Trench, "Full aperture laser conditioning of multilayer mirrors and polarizers," Proc. SPIE **2633**, 457–463 (1995).
7. F. Y. Génin, C. J. Stolz, and M. R. Kozlowski, "Growth of laser-induced damage during repetitive illumination of HfO_2/SiO_2 multilayer mirror and polarizer coatings," Proc. SPIE **2966**, 273–282 (1997).
8. X. F. Liu, X. Li, D. W. Li, Y. A. Zhao, and J. D. Shao, "An automated damage diagnostic system for laser damage threshold tests," Chin. Opt. Lett. **8**, 407–410 (2010).
9. X. F. Liu, D. W. Li, Y. A. Zhao, X. Li, X. L. Ling, and J. D. Shao, "Damage characteristics of HfO_2/SiO_2 45° incidence high reflector in 1-on-1 and N-on-1 tests," Chin. Opt. Lett. **8**, 41–44 (2010).
10. J. Hue, F. Y. Génin, and S. Maricle, "Comparison of the single pulse delaminate damage size for 3 ns and 10 ns pulses," Lawrence Livermore National Laboratory report (12 June 1996).
11. X. F. Liu, D. W. Li, Y. A. Zhao, and X. Li, "Further investigation on the damage characteristic of nodular defects," Appl. Opt. **49**, 1774–1779 (2010).
12. H. Y. Hu, Z. X. Fan, and Y. Liu, "Measuring weak absorptance of thin film coatings by surface thermal lensing technique," Laser Phys. **10**, 633–639 (2000).
13. A. L. Rigatti and D. J. Smith, "Status of optics on the OMEGA laser after 18 months of operation," Proc. SPIE **2966**, 441–450 (1997).
14. C. J. Stolz, M. D. Feit, and T. V. Pistor, "Laser intensification by spherical inclusions embedded within multilayer coatings," Appl. Opt. **45**, 1594–1601 (2006).
15. Y. G. Shan, H. B. He, C. Y. Wei, S. H. Li, M. Zhou, D. W. Li, and Y. A. Zhao, "Geometrical characteristics and damage morphology of nodules grown from artificial seeds in multilayer coating," Appl. Opt. **49**, 4290–4295 (2010).
16. M. Ushio, K. Komurasaki, K. Kawamura, and Y. Arakawa, "Effect of laser supported detonation wave confinement on termination conditions," Shock Waves **18**, 35–39 (2008).
17. E. Stormer and M. von Allmen, "Influence of laser-supported detonation waves on metal drilling with pulsed CO_2 lasers," J. Appl. Phys. **49**, 5648–5654 (1978).
18. A. Salleo, T. Sands, and F. Y. Génin, "Machining of transparent materials using an IR and UV nanosecond pulsed laser," Appl. Phys. A **71**, 601–608 (2000).